

Human umbilical cord-derived mesenchymal stem cells promote repair of neonatal brain injury caused by hypoxia/ischemia in rats

<https://doi.org/10.4103/1673-5374.339002>

Date of submission: May 2, 2021

Date of decision: July 4, 2021

Date of acceptance: December 11, 2021

Date of web publication: April 1, 2022

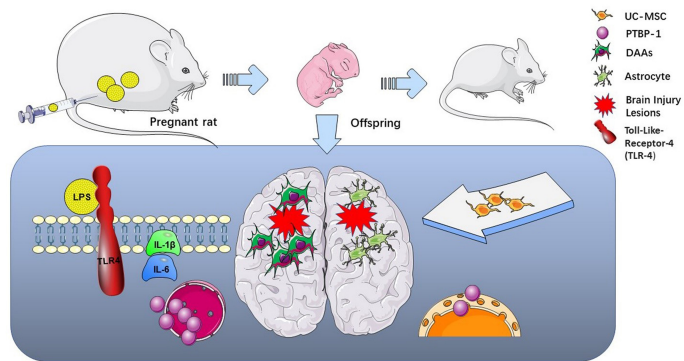
Yang Jiao^{1,2,3}, Yue-Tong Sun⁴, Nai-Fei Chen⁴, Li-Na Zhou^{1,3}, Xin Guan^{1,2}, Jia-Yi Wang^{1,2}, Wen-Juan Wei^{1,2}, Chao Han^{1,2}, Xiao-Lei Jiang⁴, Ya-Chen Wang^{1,2}, Wei Zou^{2,4,*}, Jing Liu^{1,2,*}

From the Contents

Introduction	2518
Materials and Methods	2519
Results	2520
Discussion	2523

Graphical Abstract

Polypyrimidine tract-binding protein-1 (PTBP-1) may be a key protein in the regulation of lipopolysaccharide (LPS)-induced maternal immune activation



Abstract

Administration of human umbilical cord-derived mesenchymal stem cells (hUC-MSCs) is believed to be an effective method for treating neurodevelopmental disorders. In this study, we investigated the possibility of hUC-MSCs treatment of neonatal hypoxic/ischemic brain injury associated with maternal immune activation and the underlying mechanism. We established neonatal rat models of hypoxic/ischemic brain injury by exposing pregnant rats to lipopolysaccharide on day 16 or 17 of pregnancy. Rat offspring were intranasally administered hUC-MSCs on postnatal day 14. We found that polypyrimidine tract-binding protein-1 (PTBP-1) participated in the regulation of lipopolysaccharide-induced maternal immune activation, which led to neonatal hypoxic/ischemic brain injury. Intranasal delivery of hUC-MSCs inhibited PTBP-1 expression, alleviated neonatal brain injury-related inflammation, and regulated the number and function of glial fibrillary acidic protein-positive astrocytes, thereby promoting plastic regeneration of neurons and improving brain function. These findings suggest that hUC-MSCs can effectively promote the repair of neonatal hypoxic/ischemic brain injury related to maternal immune activation through inhibition of PTBP-1 expression and astrocyte activation.

Key Words: developmental brain disease model; disease-associated astrocytes; intranasal administration; lipopolysaccharide; maternal immune activation; neonatal brain injury; neuroplasticity repair; polypyrimidine tract-binding protein-1; stem cell therapy; umbilical cord-derived mesenchymal stem cells

Introduction

Neonatal brain injury (NBI) is generally induced by hypoxia/ischemia, inflammation, or infection during critical periods of development. NBI can lead to long-term neurodevelopmental abnormalities, including motor impairments, mental and developmental retardation, learning disabilities, and psychiatric disorders (Li et al., 2017a; Pierrat et al., 2017). Clinical studies have shown that children born to mothers exposed to viral and bacterial pathogens during pregnancy are at higher risk of developing various neurological diseases, including cerebral palsy, schizophrenia, autism, bipolar disorder, major depression, and epilepsy (Burd et al., 2012; Mwaniki et al., 2012; Bergdolt and Dunaevsky, 2019). Experimental models have shown that lipopolysaccharide (LPS)-induced prenatal maternal immune activation (MIA) can lead to activation of astrocytes and microglia and to significant declines in the long-term neuronal plasticity of offspring (Canetta et al., 2016; Estes and McAllister, 2016).

In newborns, current research suggests that neuronal circuits involved in fine motor control, motor learning, and cognitive function are particularly susceptible to damage from systemic inflammation and hypoxia (Fragopoulou et al., 2019). Studies have consistently demonstrated that disease-associated astrocytes (DAAs) respond to inflammatory damage by promoting release of inflammatory factors, which accelerate activation of astrocytes and microglia (Chávez et al., 2019; Wang et al., 2019; Hampel et al., 2020). DAAs stimulate neuronal repair and regeneration by inducing transdifferentiation and by inhibiting release of proinflammatory cytokines (Qian et al., 2020). Astrocytes exhibit different activation states depending on functional localization, which is distinguishable by the expression levels of glial fibrillary acidic protein (GFAP) (Habib et al., 2020). Reactive astrocytes can be categorized into A1 or A2 subtypes (Vismara et al., 2020), with A1 “harmful” astrocytes leading to aggravation of brain injury and A2 “beneficial” astrocytes playing a protective role in neurons (Chen et al., 2019). Expression of A1 reactive astrocytes, or DAAs, has been shown to be induced by classically activated

¹Stem Cell Clinical Research Center, National Joint Engineering Laboratory, Regenerative Medicine Center, The First Affiliated Hospital of Dalian Medical University, Dalian, Liaoning Province, China; ²Dalian Innovation Institute of Stem Cells and Precision Medicine, Dalian, Liaoning Province, China; ³Department of Neurology, The First Affiliated Hospital of Dalian Medical University, Dalian, Liaoning Province, China; ⁴College of Life Science, Liaoning Normal University, Dalian, Liaoning Province, China

*Correspondence to: Jing Liu, PhD, liujing@dmu.edu.cn; Wei Zou, PhD, weizou60@126.com.

<https://orcid.org/0000-0002-0493-296X> (Jing Liu); <https://orcid.org/0000-0002-2203-8347> (Wei Zou); <https://orcid.org/0000-0001-8476-7978> (Yang Jiao)

Funding: This work was supported by the National Natural Science Foundation of China, No. 81471308 (to JL); Stem cell Clinical Research Registry Program, No. CMR-20161129-1003 (to JL); Liaoning Province Excellent Talent Program Project of China, No. XLYC1902031 (to JL); Dalian Innovation Fund of China, No. 2018J11CY025 (to JL); and National Defense Science and Technology New Special Zone Contract, No. 19-163-00-kx-003-001-01 (to JL).

How to cite this article: Jiao Y, Sun YT, Chen NF, Zhou LN, Guan X, Wang JY, Wei WJ, Han C, Jiang XL, Wang YC, Zou W, Liu J (2022) Human umbilical cord-derived mesenchymal stem cells promote repair of neonatal brain injury caused by hypoxia/ischemia in rats. *Neural Regen Res* 17(11):2518-2525.



neuroinflammatory microglia and can be identified by higher expression levels of GFAP (Liddel et al., 2017; Habib et al., 2020).

After brain injury, activated astrocytes have been shown to undergo *in situ* conversion into neurons through a process called transdifferentiation, with polypyrimidine tract-binding protein-1 (PTBP-1) playing a key inhibitory role in this process (Qian et al., 2020). PTBP-1 is a 57-kDa protein that binds to the polypyrimidine tract region in introns (García-Blanco et al., 1989). Recent research has suggested that these transdifferentiated cells can replace lost neurons and reconstitute endogenous neural circuits (Gascón et al., 2017). PTBP-1, which is a special, system-dependent transcription factor with *in vivo* reprogramming effects, may therefore be a key factor and therapeutic target in neurological diseases. Previous studies have confirmed PTBP-1's role in a murine model of degenerative brain diseases; however, this protein has never been studied in a developmental model of NBI (Lei et al., 2020; Qian et al., 2020; Zhou et al., 2020).

Human umbilical cord mesenchymal stem cell (UC-MSC) transplantation has been shown to be a powerful method for stimulating endogenous repair processes, leading to changes in behavioral outcomes and volumes of cerebral lesion after neonatal brain damage. Mesenchymal stem cells (MSCs) can inhibit astrocyte activation, reduce expression of inflammatory factors, and replace lost neurons (Thomi et al., 2019a; Xu et al., 2019). New developments related to intranasal administration and exosome application of stem cells have helped make this therapy even safer and more precise (Drommelschmidt et al., 2017; Thomi et al., 2019b). Although the therapeutic effects of MSC transplantation have previously been reported (Dabrowska et al., 2019), methods for achieving sustained therapeutic efficacy have not been fully developed yet.

Our study investigated whether MIA-induced NBI is regulated by activation of DAAs and by PTBP-1 expression in the attempt to find a therapeutic target that would reverse the injury process and achieve neuroplasticity repair, thereby providing evidence for investigating the mechanism of stem cell treatment.

Materials and Methods

Animals and experimental design

Four pregnant Sprague-Dawley rats (gestational days [G] 16 and 17) were obtained from the specific-pathogen-free Experimental Animal Center of Dalian Medical University (Dalian, China; SCXK2018-0003) and housed individually in standard plastic cages (Liaoning Normal University). The rats were allowed free access to food and water under controlled temperature and a 12-hour light/dark cycle. The four pregnant rats were randomly assigned to two groups: two were injected intraperitoneally with 0.5 mg/kg LPS (*Escherichia coli* O111:B4, L2630-10 mg, Sigma-Aldrich, Shanghai, China; LPS: normal saline = 1:1) and the other two were injected intraperitoneally with 0.5 mg/kg PBS on G16 and G17. In the control group, 13 pups (male:female = 8:5) were delivered by the PBS-injected pregnant rats. In the LPS + PBS group, 11 pups (male:female = 6:5) were delivered, and in the LPS + UC-MSC group, 9 pups (male:female = 5:4) were delivered. On postnatal day 1 (P1), the male and female pups participating in the study were numbered separately and randomly grouped by an individual blinded to the study groups. The randomization sequence was created using Stata 9.0 (Stata Corp., College Station, TX, USA) statistical software, which was center-stratified with a 1:1:1 allocation using random block sizes, and the grouping results were revealed on P12 before treatment. On P3–12, the growth and development of the pups were assessed. Ear standing: the rats' ears can stand up completely. If the ear edge is not attached to the coat, the result is set as positive. Righting reflex: if the young rat can successfully complete a turnover three times in a row, the result is set as positive within 3 seconds. Incisor odontogenesis: if the operator's finger touches the anterior teeth, it is positive. Auditory astonishment: a tuning fork is tapped with a predetermined force 10 cm from the ear edge of the baby mouse to make a sound. If the head of the young rat is tilted to the opposite side, or the rat controls its head to avoid facing the edge, it is considered positive. Eye opening: the newborn rat is positive when both eyes are fully opened at the same time.

On P14, pentobarbital sodium (50 mg/kg, 1 mL:0.1 g, P3761, Sigma-Aldrich) was intraperitoneally injected into rats for 10 minutes for anesthesia, and then 1×10^5 MSCs in 10 μ L (~5 μ L were injected into each nasal cavity) of normal saline were intranasally administered to 11 rat pups randomly selected from the LPS group (LPS + UC-MSCs group). At the same time, PBS (10 μ L) was delivered intranasally to rat pups allocated to the LPS + PBS group (Figure 1A). The animal experiment protocol was approved by the Animal Ethics Committee of Liaoning Normal University (approval No. LL2020007) on December 14, 2020.

Isolation and identification of UC-MSCs

Umbilical cord specimens were provided by the Department of Obstetrics, The First Affiliated Hospital of Dalian Medical University. These specimens were taken from healthy fetuses delivered by cesarean section. Pregnant women and family members signed written informed consent (Additional File 1) for this process. The use of human tissue was approved by the Ethics Committee of The First Affiliated Hospital of Dalian Medical University (No. LCKY2016-59) on November 16, 2016.

Human UC-MSCs were extracted using the tissue block adherence method (Dominici et al., 2006). Within 24 hours, the umbilical cord, which was stored

under aseptic conditions at 4°C, was cleaned and cut into 1–3 mm³ segments in PBS containing 1% tri-antibody (C0223, 100 mL, Beyotime, Shanghai, China), and then soaked in a special medium of amniotic mesenchymal stem cells (Beijing Tongli Haoyuan Biotechnology Co., Ltd., Beijing, China). Wharton's jelly was placed face down on a 10-cm petri dish. After 20 minutes, 10 mL of culture medium was added, and the dish was placed in an incubator containing 5% CO₂ at 37°C. The medium was changed every 3 days. After the cells were passaged five times, when they reached 80–90% confluence, they were used for flow cytometry.

Single cell suspensions of UC-MSCs in PBS were incubated with mouse anti-human CD73-BV421 (BD Pharmingen, Franklin Lakes, NJ, USA, Cat# 562430, RRID: AB_11153119), mouse anti-human CD105-APC (BD Pharmingen, Cat# 562408, RRID: AB_11154045), mouse anti-human CD90-fluorescein isothiocyanate (FITC) (BD Pharmingen, Cat# 555595, RRID: AB_395969), mouse anti-human HLA-DR-PE (BD Pharmingen, Cat# 555812, RRID: AB_396146), mouse anti-human CD34-PerCP-Cy^{5.5} (BD Pharmingen, Cat# 347203, RRID: AB_400266), or mouse anti-human CD45-FITC (BD Pharmingen, Cat# 555482, RRID: AB_395874) for 25 minutes at 4°C. After two washes, the cells were resuspended in PBS. Fluorescence-activated cell sorting (FACS) analyses were performed using a Flow Cytometer (BD LSRFortessa, BD Biosciences).

Tissue preparation

On P40, pups were deeply anesthetized by an intraperitoneal injection of 1% pentobarbital sodium (50 mg/kg). For western blot analysis, after rapidly removing the brain, the areas of interest were dissected and stored at –80°C. For hematoxylin and eosin staining, Nissl staining, immunohistochemistry, and immunofluorescence, pup brains were perfusion-fixed with 4% paraformaldehyde, dehydrated with a 30% sucrose solution, and embedded in optimal cutting temperature compound for frozen sectioning, with a slice thickness of 4 μ m. Starting from the same part of the brain tissue in each group, each slice of every 10 brain slices was selected for comparison to avoid subjective underestimation of the number of positive cells.

Hematoxylin and eosin and Nissl staining

Slices were washed with distilled water, stained with hematoxylin for 5 minutes, and then stained with eosin for 5 minutes. Alcohol, xylene, and neutral adhesives were used for dehydration, transparency, and sealing, respectively. Sections were removed from 4°C and left at room temperature for 30 minutes. They were then washed with double distilled water and a filtered tar violet solution was added for 2 hours. The sections were then rinsed three times with water for 3 minutes and observed using a light microscope (CH-2, Olympus, Tokyo, Japan). For counterstaining, sections were sequentially dehydrated in 70%, 80%, and 95% alcohol solutions. Sections were then destained in a 1% hydrochloric acid alcohol destaining solution and placed in a 100% alcohol solution followed by xylene for 5 minutes each. Sections were then taken out to dry and sealed with a neutral resin, after which the neutral gum was completely air-dried and observed under a light microscope.

Immunohistochemistry and immunofluorescence staining

Immunohistochemical staining

Brain tissue was fixed with 4% paraformaldehyde, embedded in paraffin, and cut into 4- μ m sections. The sections were deparaffinized in xylene, and then rehydrated using an alcohol gradient. Next, the sections were incubated overnight with an anti-PTBP-1 antibody (1:150; rabbit, Abcam, Cambridge, UK, Cat# ab133734) at 4°C, and then incubated with a secondary antibody (1:100; goat, Thermo Fisher Scientific, Fremont, CA, USA, Cat# TL-125-QHL) at 25 \pm 1°C for 30 minutes, followed by incubation with a diaminobenzidine tetrachloride solution at 25 \pm 1°C for 1 minute and counterstaining with Mayer's hematoxylin. Images were captured using an optical microscope (Olympus).

Immunofluorescence staining

Frozen brain tissue sections were fixed by incubation with cold acetone for 30 minutes, and then permeabilized by incubation with 0.5% Triton X-100 in PBS for 10 minutes at 25 \pm 1°C. Tissue sections were incubated overnight at 4°C with different primary antibodies, including anti-interleukin (IL)-1 β (1:50; rabbit, Abcam, Cat# ab254360) and anti-IL-6 (1:200; mouse, Abcam Cat# ab9324, RRID: AB_307175), followed by secondary antibodies with different fluorescent conjugates including FITC (1:2000, goat, Abcam, Cat# ab6785, RRID: AB_955241) and Alexa Fluor 647 (1:1000, donkey, Abcam, Cat# ab150075, RRID: AB_2752244) at 25 \pm 1°C for 30 minutes. After 4',6-diamidino-2-phenylindole staining, sections were visualized using a fluorescence microscope (Olympus FV1000) and digital images were captured using FV10-ASW 3.1 software.

Brain tissue slices on slides were deparaffinized and rehydrated, blocked with 5% bovine serum albumin, incubated with antibodies for PTBP-1 (1:150; rabbit, Abcam, Cat# ab133734) and GFAP (1:200; mouse, Servicebio, Wuhan, China, Cat# servicebio-GB12096), and then with secondary antibodies conjugated to FITC (1:2000, goat, Abcam, Cat# ab6785, RRID: AB_955241) or Alexa Fluor 647 (1:1000, donkey, Abcam, Cat# ab150075, RRID: AB_2752244). After 4',6-diamidino-2-phenylindole staining, the slides were observed using a fluorescence microscope (Olympus FV1000). Digital images were captured using FV10-ASW 3.1 software, and the purity of neurons was measured by Image Pro Plus 6.0 software (Media Cybernetics, Annapolis, MD, USA).

Western blot assay

For western blot analysis, the hippocampus and cortical tissue of rats were dissected on P40 and total protein was extracted in radioimmunoprecipitation assay lysis buffer (Beyotime Biotechnology, Haimen, China) containing protease inhibitors (1:100, Beyotime Biotechnology). Protein concentrations were determined using the bicinchoninic acid assay (Thermo Fisher Scientific, Waltham, MA, USA). Equal amounts of protein (50 µg) were separated using sodium dodecyl sulfate-polyacrylamide gel electrophoresis (Thermo Fisher Scientific) with a 10% gel and transferred to polyvinylidene difluoride membranes (Roche, Mannheim, Germany, Cat# 03010040001). The membranes were blocked with 5% skim milk for 2 hours at 25 ± 1°C and incubated overnight with anti-GFAP (1:10,000; mouse, Abcam, Cat# ab7260, RRID: AB_305808), anti-PTBP-1 (1:10,000; rabbit, Abcam, Cat# ab133734, RRID: AB_2814646), anti-neuron-specific class III β-tubulin (TUJ-1; 1:1000; mouse, Abcam, Cat# ab78078, RRID: AB_2256751), or anti-β-actin antibodies (1:1000; mouse, Abcam, Cat# ab8226, RRID: AB_306371), followed by incubation with horseradish peroxidase-conjugated secondary antibodies (1:10,000, Abbkine Inc., Wuhan, China, Cat# A21020 [goat], RRID: AB_2876889/A25112 [goat]) for 2 hours at 25 ± 1°C. Immunoreactive bands were visualized using enhanced chemiluminescence (WBKLS0100, Millipore, Shanghai, China) and the optical intensity of the bands was analyzed using Image-Pro Plus 6.0 (Media Cybernetics).

Behavioral tests

Open field test

P28 pups were placed in the bottom center of a reaction chamber and a camera (FP800, Panasonic, Xiamen, China) was turned on to record the total moving distance, surrounding moving distance, surrounding moving time, center moving distance, center moving time (then obtain the average distance and time), and the motion trajectory of each pup within 300 seconds (Sturman et al., 2018). After the experiment was completed, the inner and bottom surfaces of the reaction chamber were cleaned in the open air to prevent residual information from affecting future test performances. The experimental environment was kept quiet, and the temperature and humidity were appropriate and stable to reduce the effects of environmental factors on the behavior of the experimental animals. An open field experiment platform and a SuperMaze Animal Behavior Video Analyzer were provided by Shanghai Newsoft Co., Ltd. (Shanghai, China).

Morris water maze test

The Morris water maze test was used to evaluate the spatial learning and memory abilities of rats (Cui et al., 2017). According to previous studies, P28 rat pups were trained to find hidden underwater platforms (Shanghai Newsoft Co., Ltd.) three times per day for 3 days. The escape latency was recorded to assess the pups' learning ability. On the fourth day, a formal test was conducted, with a 60-second delay time for finding the hidden platform; the total distance and number of target crossings were recorded for a comprehensive evaluation of the learning and memory ability and the spatial positioning ability (Ravichandran et al., 2018; Muhammad et al., 2019).

Balance beam test

The balance beam (Shanghai Newsoft Co., Ltd.) was a standard square and round horizontal beam (1 m × 5 cm × 5 cm) placed at a height of 50 cm. The balance beam was divided into two parts, a square wooden section that was easy to cross, and logs, which were harder to cross. After three consecutive training sessions on P28, rat pups were able to cross within 20 seconds. During the formal experiment, the number of left and right hindlimb drops while crossing the square or round balance beam was separately recorded to assess the balance ability of the young rats. After each test, the balance beam was cleaned with alcohol to prevent any odor from interfering with subsequent testing (Faezi et al., 2018).

Statistical analysis

No statistical methods were used to predetermine sample sizes; however, our sample sizes were similar to those reported in previous publications (Jiao et al., 2019, 2021). No animals or data points were excluded from the analysis (the evaluator was blind to the grouping results). The data are presented as the mean ± standard error of the mean (SEM) and were analyzed using SPSS 18.0 (SPSS Inc., Chicago, IL, USA). One-way analysis of variance followed by the Student-Newman-Keuls method was applied to analyze differences among groups. $P < 0.05$ was considered statistically significant.

Results

UC-MSCs identification

UC-MSCs were subcultured from passage 3 according to the method described above and were in good growth condition for flow cytometry analysis. After incubation with CD73, CD105, CD90, HLA-DR, CD34, or CD45 antibodies, flow cytometry showed the following expression patterns on the surface of isolated and cultured human UC-MSCs: CD73, CD105, and CD90 were expressed at 99.94%, 98.62%, and 99.86%, respectively, whereas HLA-DR, CD34, and CD45 showed expression rates of 0.13%, 0.36%, and 0.18%, respectively. These results indicated that the stem cells we cultured met the identification criteria for UC-MSCs (Dominici et al., 2006) (Figure 1A).

UC-MSCs attenuate the morphological and behavioral abnormalities of the rat model of MIA-associated NBI

MIA-related NBI affects the ontogeny and brain morphology of neonatal rats

All 13 rats in the control group survived, whereas one of the 12 rats in the

LPS + PBS group died on P31. Two of the 11 pups in the LPS + UC-MSC group died showing excessive anesthesia (0.4 mL/100 g) and pulmonary infection in the autopsy. Body weight measured every 3 days did not differ between the control and LPS (LPS + PBS/LPS + UC-MSC) groups (P3: $P = 0.153$, P6: $P = 0.090$, P9: $P = 0.061$, P12: $P = 0.090$; Figure 1B).

We compared the growth and development of the newborn rats. All pups (control and LPS groups) were tested for ear setting, righting reflex, incisor generation, auditory astonishment, and eye opening. The results suggest that injection of LPS during pregnancy did not affect the overall developmental time and weight (Figure 1C).

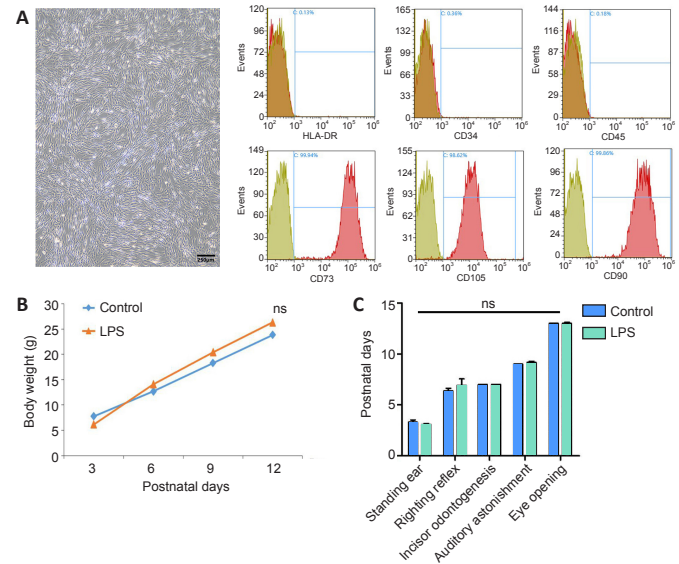


Figure 1 | Experimental flowchart and growth and development of newborn pups with maternal immune activation-associated neonatal brain injury.

(A) Cell morphology and surface markers of passage 5 cells. Umbilical cord mesenchymal stem cells were spindle-shaped. CD73, CD105, and CD90 staining was positive, with positive expression rates of 99.94%, 98.62%, and 99.86%, respectively. HLA-DR, CD34, and CD45 showed expression rates of 0.13%, 0.36%, and 0.18%, respectively. Scale bar: 250 µm. (B) Neonatal rat weight was measured every 3 days. (C) Assessment of developmental indicators of neonatal rats. The pups were tested for ear standing, righting reflex, incisor odontogenesis, auditory astonishment, and eye opening. Data are expressed as mean ± SEM (control: $n = 13$, LPS + PBS: $n = 11$, LPS + UC-MSC: $n = 9$). ns: Not significant, vs. control group (one-way analysis of variance followed by the Student-Newman-Keuls method). LPS: Lipopolysaccharides; P: postnatal day; PBS: phosphate-buffered saline; UC-MSCs: umbilical cord-derived mesenchymal stem cells.

Using hematoxylin and eosin staining, we examined the morphological changes in the cortex and hippocampus of pups in the prenatal LPS-induced model of brain injury (Figure 2A and B). Compared with the control group, the LPS pups had cavities in the cerebral cortex and hippocampal regions CA1, CA3, and dentate gyrus (DG), demonstrating a loose arrangement, with neuronal cell shrinkage, chromatin condensation, partial nuclear pyknosis, nuclear fragmentation, nucleolar blurring and even disappearance, and capillary zone expansion (Figure 2B). These findings suggest that injection of LPS into the mothers caused MIA-related brain damage in the offspring.

UC-MSCs relieve cerebral tissue pathological changes in the rat model of MIA-associated NBI

We studied the recovery of brain injury sites after intranasal administration of UC-MSCs (Figure 3). Nissl staining showed that in the LPS + UC-MSC group, the cortical and hippocampal neuronal damage was alleviated. Neurons in the cortex and hippocampus of these offspring were significantly stained, with evidence of more clearly arranged cell layers (Figure 3). This finding suggests that while LPS injection affected the morphological development of main functional areas in the rat brain, administration of UC-MSCs improved the survival of nerve cells after brain injury in these young rats.

UC-MSCs improve the exploration and balance in the rat model of MIA-associated NBI

To investigate the effects of MIA injury and UC-MSC treatment on spontaneous activity behavior or exploratory behavior, the learning, memory, and balance abilities of pups with brain injury were examined by behavioral evaluations on P28. In the open field test, the movement trajectory of rats in the LPS + PBS group was significantly decreased compared with the control group ($P = 0.000$; Figure 4C); however, the average moving distance and duration were not significantly different (Figure 4A and B). After intranasal administration of UC-MSCs, the movement distance of pups in the surrounding distance significantly increased ($P = 0.000$). Furthermore, the walking distance in the central area was significantly shorter after LPS injection (LPS + PBS and LPS + UC-MSC groups) compared with the control group ($P = 0.000$). Compared

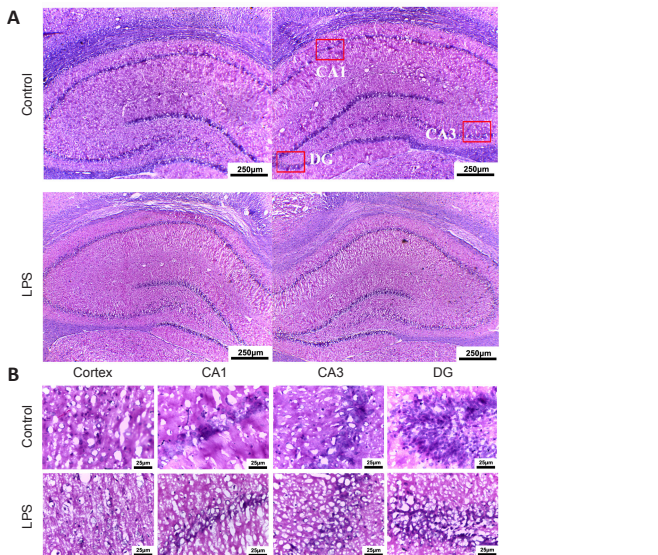


Figure 2 | Pathological changes in the brain of neonatal rats with maternal immune activation-associated neonatal brain injury (hematoxylin and eosin staining).

(A) Pathological changes in neonatal rats' hippocampus (original magnification 40x, scale bars: 250 μm). The cortical cells in the LPS group had obvious nucleoli, the number of cells was significantly reduced, and the arrangement was loose, showing a "vacuum" appearance. The hippocampal structure in the control group was more intact and cells were lined up more neatly. (B) Pathological changes in the cortex and hippocampal CA1, CA3, and DG (original magnification 200x, scale bars: 25 μm). Compared with the control group, the number of neurons in the brain cortex and hippocampus of young rats in the LPS group was significantly reduced. The neuronal nuclei were deeply stained and the nucleoli disappeared. Moreover, the neuronal structure was loose and lacked hierarchy. DG: Dentate gyrus; LPS: lipopolysaccharides; PBS: phosphate-buffered saline; UC-MSCs: umbilical cord-derived mesenchymal stem cells.

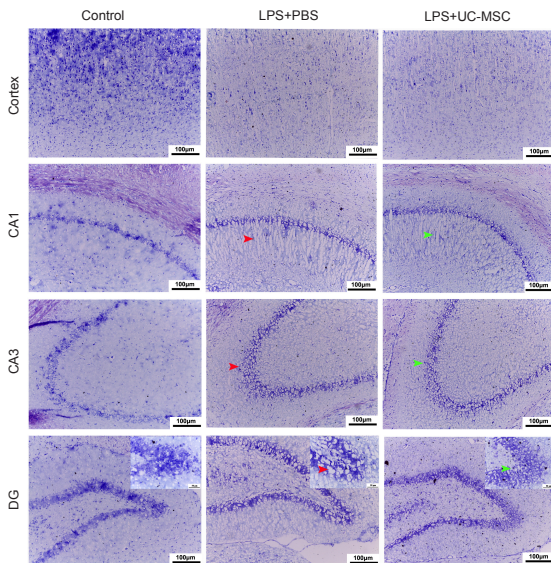


Figure 3 | Effect of UC-MSCs on the pathological changes in the brain tissue of neonatal rats with maternal immune activation-associated neonatal brain injury.

The widened pericapillary space and cerebral edema (red arrow) was observed in the cortex, CA1, CA3, and DG areas (Nissl staining, original magnification 200x, scale bars: 100 μm; original magnification in the enlarge parts 400x, scale bars: 50 μm). After intranasal hUC-MSCs administration, the neuronal structure was relatively clear. Stromal edema was reduced (green arrow). The number of neurons in the cerebral cortex of young rats in the LPS group was less than that in the control group, and the structure was loose. DG: Dentate Gyrus; LPS: lipopolysaccharides; PBS: phosphate-buffered saline; UC-MSCs: umbilical cord-derived mesenchymal stem cells.

with the LPS + PBS group, the movement trajectory of pups in the LPS + UC-MSC group was increased in the open field test and the exploration trajectory in the center area was prolonged (Figure 4C).

In the Morris water maze test, we found that compared with the control group, pups in the LPS group required more time to learn where to find the platform during the 3-day training phase, especially during the first day of training ($P = 0.000$; Figure 4D). Additionally, the escape latency of the LPS + UC-MSC group was slightly shorter in the first two days compared with that of the LPS + PBS group, but the difference was not statistically

significant. In the formal testing, the pups in the LPS + UC-MSC group found the platform correctly more frequently, and the total distance of searching the platform was slightly shorter compare with the LPS + PBS group, however the differences were not significant ($P = 0.423$; Figure 4E). Furthermore, the number of successful platform crossing contact in the Morris water maze test of the LPS + UC-MSC group improved compared with that of the control group ($P = 0.014$; Figure 4F), but not compared with the LPS + PBS group ($P = 0.244$). However, this number also improved in the LPS + PBS group compared with the control group ($P = 0.022$).

The balance beam test revealed that the control pups could quickly pass through the wide square balance beam without hindlimb drops, whereas pups in the LPS + PBS group showed hindlimb drops (Figure 4G; $P = 0.006$). However, in the more difficult round balance beam test, there were no significant differences in hindlimb drops between the control and LPS + PBS groups ($P = 0.095$) and between the LPS + PBS and LPS + UC-MSC groups ($P = 0.799$). These results suggest that UC-MSC treatment improved the cognitive, learning, and memory impairments caused by LPS injection during pregnancy in young rats, especially fast learning and memory. However, the effects of this treatment on motor exploration and balance of neonatal rats are still unclear and need further research.

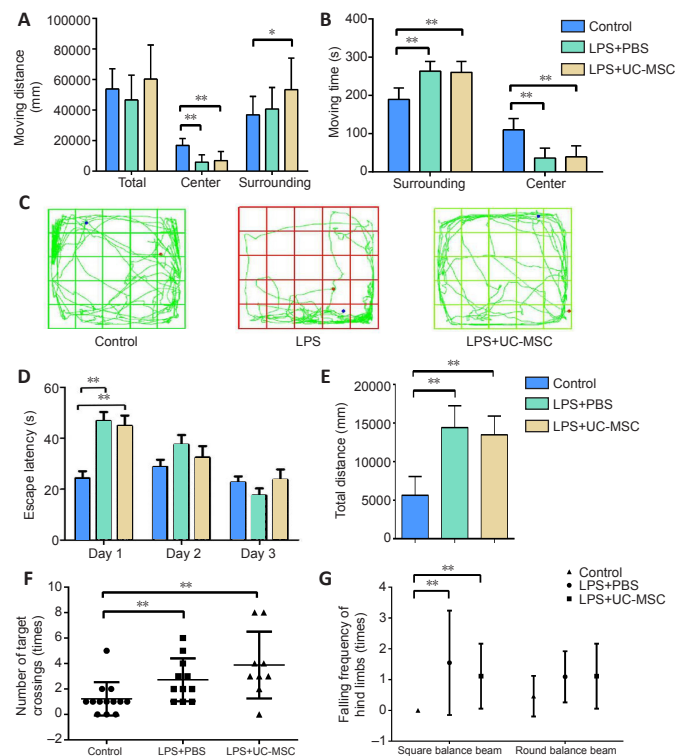


Figure 4 | Effect of UC-MSCs on behavioral tests of neonatal rats with maternal immune activation-associated neonatal brain injury.

(A–C) The movement distance (total, center, surrounding) (A), total moving time (B), and movement trajectory (C) in the open field test. Blue dots indicate the starting point of the test, red dots indicate the end point of the test, and green lines indicate the trajectory. (D) Escape latency in the Morris water maze training stage on the training days. (E) The total distance to search for the platform in the Morris water maze formal test on the fourth day. (F) The number of successful platform crossings in the Morris water maze formal test. Data are expressed as mean ± SEM (control: $n = 13$, LPS + PBS: $n = 11$, LPS + UC-MSC: $n = 9$). * $P < 0.05$, ** $P < 0.01$ (one-way analysis of variance followed by the Student-Newman-Keuls method). (G) The number of drops of left or right leg in the square/round balance beam test. LPS: Lipopolysaccharides; MWM: Morris water maze; PBS: phosphate-buffered saline; UC-MSCs: umbilical cord-derived mesenchymal stem cells.

Astrocyte activation is related to MIA-associated NBI, and UC-MSC treatment suppresses DAAs in neonatal rats

Expression levels and distribution patterns of GFAP

We performed immunofluorescence to determine the expression levels and distribution patterns of MIA-related GFAP-positive astrocytes in the brain. Immunofluorescence staining showed that many activated astrocytes infiltrated and synaptic extensions were clearly seen in the cortex of newborn rats affected by LPS during pregnancy, with a similar pattern in the CA1, CA3, and DG areas of the hippocampus. However, the fluorescence intensity of GFAP-positive activated astrocytes in the cortex and hippocampus was decreased after UC-MSC treatment (Figure 5A–D). In the cortex, GFAP-positive activated astrocytes were arranged in a centripetal layer after MIA injury. In the hippocampus, GFAP-positive astrocytes were dispersed around hippocampal neurons in the damaged area, with a relatively uniform distribution pattern (Figure 5). In the UC-MSC group, GFAP-positive astrocytes showed a more regular linear arrangement along the specific entorhinal cortex (EC) projection pathway, with the anatomical structure suspected to align with the perforant path/CA1 indirect pathway (Figure 5).

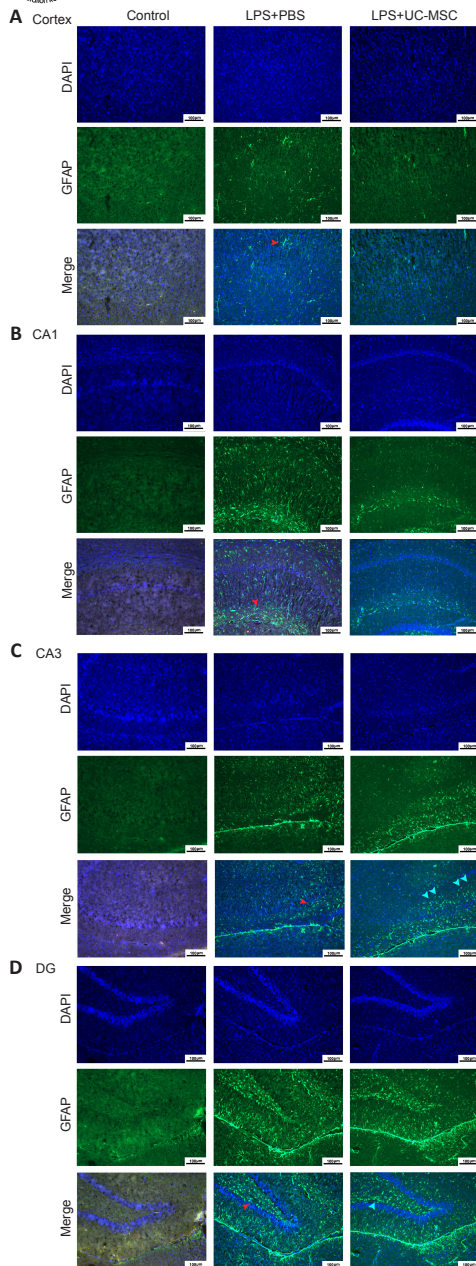


Figure 5 | Effects of UC-MSCs on the distribution of GFAP-positive DAAs in the cerebral cortex (A) and hippocampus CA1 (B), CA3 (C), and DG (D) of neonatal rats with maternal immune activation-associated neonatal brain injury (immunofluorescence).

In the LPS + PBS group, the GFAP (green, stained by FITC)-positive activated astrocytes (red arrows) located in the cortex were arranged in a centripetal pattern and were more evenly distributed in the hippocampus CA1, CA3, and DG. In the LPS + UC-MSC group, GFAP-positive activated astrocytes were densely distributed along the hippocampal projection pathway (green arrow). Original magnification 100 \times , scale bars: 100 μ m. DAPI: 4',6-Diamidino-2-phenylindole; DG: dentate gyrus; GFAP: glial fibrillary acidic protein; LPS: lipopolysaccharides; PBS: phosphate-buffered saline; UC-MSCs: umbilical cord-derived mesenchymal stem cells.

Immunopositivity of inflammatory factors in different functional brain regions

As shown in **Figure 6**, immunofluorescence was used to determine the immunopositivity of the inflammatory factors, IL-6 and IL-1 β . In the LPS + PBS group, IL-6 and IL-1 β were both highly expressed in the cortex, and IL-1 β immunopositivity was slightly enhanced in the hippocampus. However, UC-MSC treatment reduced IL-6 expression in the cortex and IL-1 β expression in the cortex and hippocampus.

Low expression of PTBP-1 is related to neuron regeneration and repair

Using an immunohistochemical method we examined the expression levels and distribution patterns of PTBP-1 in various parts of the brain in each group (**Figure 7A and B**). Compared with the control group, PTBP-1 was highly expressed in the LPS + PBS group (cortex: $P = 0.018$, CA1: $P = 0.011$). In the cortex, PTBP-1 was abundantly expressed in the cell bodies of neurons and around neurons, with PTBP-1-positive cells distributed in a centripetal layer. Compared with the LPS + PBS group, PTBP-1 expression was decreased in the LPS + UC-MSC group ($P = 0.002$), with a more orderly arrangement of PTBP-1-negative neurons. In the CA1 region, PTBP-1 expression was decreased

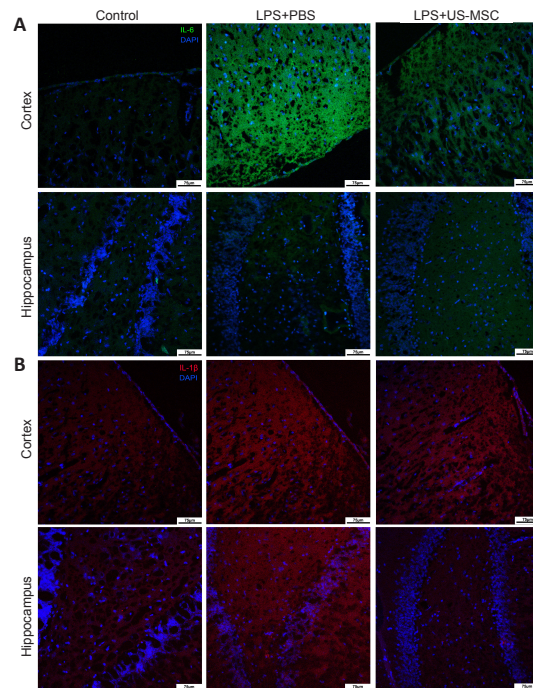


Figure 6 | Effects of UC-MSCs on the immunopositivity of inflammatory cytokines IL-6 (A) and IL-1 β (B) in the cerebral cortex and the hippocampus of neonatal rats with maternal immune activation-associated neonatal brain injury (immunofluorescence).

IL-6 (green, stained with FITC) was highly expressed in the cortex of the LPS + PBS group. In the LPS + UC-MSC group, the immunopositivity of IL-6 in the cortex was lower than that in the LPS + PBS group. There was no significant difference between these groups in the immunopositivity of IL-6 in the hippocampus. Compared with the control group, IL-1 β expression (red, stained with Alexa Fluor 647) was higher in the cortex and hippocampus of the LPS + PBS group. In the PBS + UC-MSC group, the immunopositivity of IL-1 β in the cortex was similar to that in the LPS + PBS, whereas in the hippocampus it was lower. Original magnification 100 \times , scale bars: 75 μ m. DAPI: 4',6-Diamidino-2-phenylindole; DG: dentate gyrus; IL-1 β : interleukin-1 β ; IL-6: interleukin-6; LPS: Lipopolysaccharides; PBS: phosphate-buffered saline; UC-MSCs: umbilical cord-derived mesenchymal stem cells.

in the LPS + UC-MSC group compared with that in the LPS + PBS group ($P = 0.003$), with PTBP-1-positive cells having a more orderly arrangement and mainly distributed around damaged neurons. After LPS-induced injury, PTBP-1-positive cells in CA1, CA3, and DG showed a linear distribution along the hippocampal circuit.

Next, we used immunofluorescence to examine the distribution of GFAP-positive and PTBP-1-positive cells (**Figure 8**). GFAP-positive cells ($P = 0.034$) and GFAP/PTBP-1-positive cells ($P = 0.011$) were significantly increased in the LPS + PBS group compared with the control group, but after UC-MSC treatment, the number of both cell types decreased. In the LPS + PBS group, GFAP/PTBP-1-positive cells were linearly arranged, and PTBP-1 was expressed in the nuclei of injured neurons. In the LPS + UC-MSC group, the expression level of GFAP was reduced ($P = 0.003$), and the number of GFAP/PTBP-1-positive cells was reduced compared with the LPS + PBS group ($P = 0.007$). Though these cells still showed a linear arrangement, the arrangement was looser.

We also used western blot analysis to determine the expression levels of GFAP, PTBP-1, and TUJ-1 in the cortex and hippocampus of pups after inflammatory injury and UC-MSC therapy. Compared with the control group, the protein expression levels of GFAP ($P = 0.041$) and PTBP-1 ($P = 0.002$) were significantly increased in the cortex of the LPS + PBS group. In contrast, compared with the LPS + PBS group, the protein expression levels of GFAP ($P = 0.040$) and PTBP-1 ($P = 0.019$) were significantly decreased in the cortex of the LPS + UC-MSC group. Additionally, the GFAP protein expression levels showed a decreasing trend in the hippocampus of the LPS + PBS ($P = 0.001$) and LPS + UC-MSC groups ($P = 0.000$), compared with the control group. Furthermore, the PTBP-1 expression levels showed an increasing trend in the hippocampus of the LPS + PBS group, compared with the control ($P = 0.031$), whereas in the hippocampus of the LPS + UC-MSC group they were lower than those in the LPS + PBS group ($P = 0.045$; **Figure 9A and B**).

Finally, the protein expression of TUJ-1, which is involved in neuronal regeneration, was higher in the cortex of the LPS + PBS group than that in the control group ($P = 0.025$; **Figure 9C**). Additionally, compared with the LPS + PBS group, TUJ-1 expression was significantly higher after UC-MSC treatment ($P = 0.012$), suggesting that neurons treated with MSCs were in a state of regeneration after DAA activation. Moreover, after UC-MSC treatment, TUJ-1 expression in the hippocampal injury area showed an increasing trend compared with the LPS + PBS ($P = 0.573$) and control groups ($P = 0.189$); however, the differences among the groups were not statistically significant (**Figure 9C**).

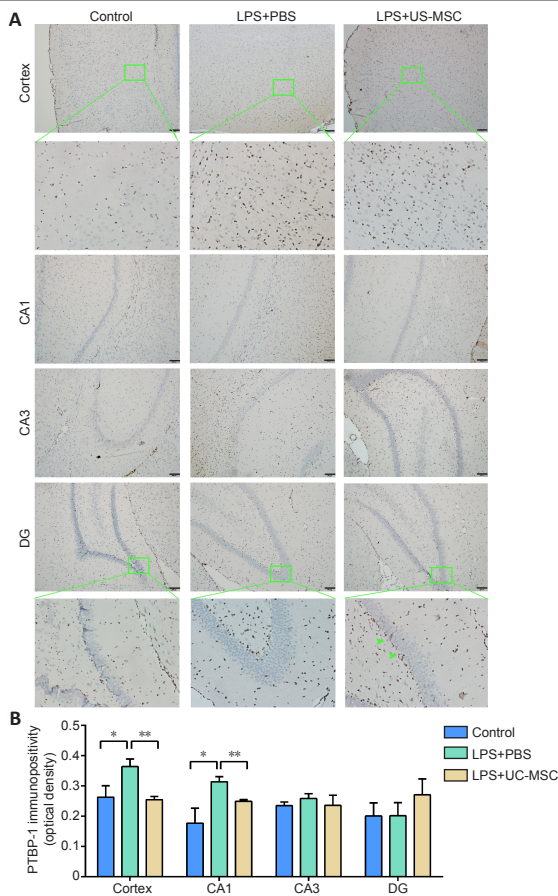


Figure 7 | Effect of UC-MSCs on the immunopositivity and distribution of PTBP-1 in various areas of the brain of neonatal rats with maternal immune activation-associated neonatal brain injury.

(A) The distribution of PTBP-1 (green arrows) in the cerebral cortex and hippocampal CA1, CA3, and DG (scale bars: 100 μ m; 50 μ m in enlarged parts). Cortex: under low magnification, the expression level of PTBP-1 protein in the LPS + PBS group was higher than that in the control group. After UC-MSCs administration, the expression level of PTBP-1 protein, compared with the LPS + PBS group, was lower. Under high magnification (green framed field), PTBP-1 was abundantly expressed in neurons and cell bodies around neurons, and PTBP-1-positive cells were distributed centripetally along the cortex. Hippocampus: under low magnification, the expression of PTBP-1 in the hippocampal CA1 area of the LPS + PBS group was higher than that in the control group and LPS + UC-MSC group. There was no significant difference between the control group, LPS + PBS group, and LPS + UC-MSC group in hippocampal CA3 and DG areas. Under high magnification, the PTBP-1-negative cells in the DG zone were loosely arranged and swollen in the LPS + PBS group; compared with the LPS + PBS group, the PTBP-1-positive cells and PTBP-1-negative cells in the UC-MSC group, were arranged more neatly and mainly distributed around the damaged neurons (green arrow). (B) Quantitative results of PTBP-1 immunopositivity. Data are expressed as mean \pm SEM ($n = 3$). * $P < 0.05$, ** $P < 0.01$ (one-way analysis of variance followed by the Student-Newman-Keuls method). DAPI: 4', 6-Diamidino-2-phenylindole; DG: dentate gyrus; LPS: Lipopolysaccharides; PBS: phosphate-buffered saline; PTBP-1: Polypyrimidine tract-binding protein-1; UC-MSCs: umbilical cord-derived mesenchymal stem cells.

Discussion

Prenatal MIA caused by infection during pregnancy can cause acute and chronic changes in the structure and function of the fetal central nervous system (Estes and McAllister, 2016). Significant associations have been identified between NBI caused by infection during pregnancy and increased risks of schizophrenia (Brown, 2011), bipolar disorder (Canetta et al., 2014), and cerebral palsy (Harvey and Boksa, 2012). MIA-related brain injury is closely related to excessive activation of astrocytes and oligodendrocytes (Burda et al., 2016; Imai et al., 2018). The occurrence and progression of MIA-induced NBI may be associated with the state and extent of astrocyte activation in specific areas (e.g., cortical and hippocampal projection circuits) at different time periods (Purves-Tyson et al., 2021). In the hippocampal region, astrocytes have been found along the same continuous trajectories, spanning from GFAP-low to GFAP-high states over six degrees in wild type mice (lower) and young Alzheimer's disease mice (higher) (Habib et al., 2020). In this study, using immunofluorescence we demonstrated that astrocytes with high GFAP expression levels were located in LPS-induced damaged cortex and hippocampal projection areas and were similar in morphology to DAAs, which validated this phenomenon in animal models of brain injury development (Purves-Tyson et al., 2021).

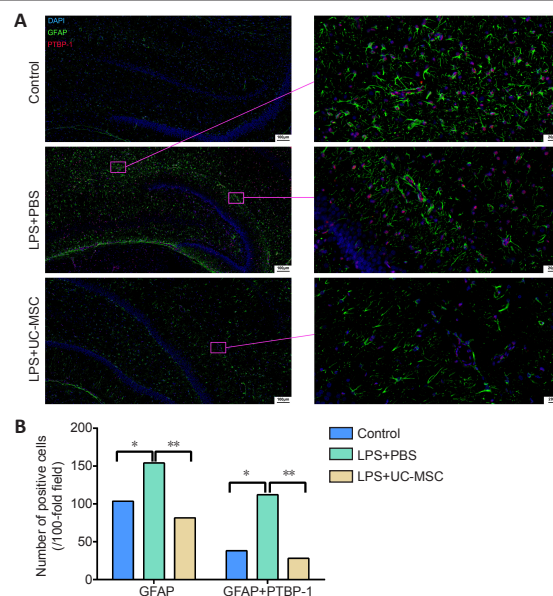


Figure 8 | Effect of UC-MSCs on the distribution of GFAP and PTBP-1-positive cells in the hippocampus of neonatal rats with maternal immune activation-associated neonatal brain injury.

(A) Immunofluorescence images of the distribution of PTBP-1 (red, stained with Alexa Fluor 647) and GFAP (green, stained with FITC) positive cells in the hippocampus. The number of GFAP-positive/PTBP-1-positive cells in the LPS + PBS group was significantly higher than that in the control group, showing a linear arrangement. In the LPS + UC-MSC group, the number of GFAP-positive/PTBP-1-positive cells was lower than that in the LPS + PBS group. Linear arrangement was still observed, but the arrangement was looser. After LPS injury, PTBP-1 was expressed in the nucleus of the injured neurons, and GFAP surrounded the PTBP-1-positive cells. Scale bars: 100 μ m (left), 20 μ m (right). (B) Quantitative results of the number of GFAP-positive cells and PTBP-1/GFAP-positive cells in the hippocampus. Data are expressed as mean \pm SEM ($n = 3$). * $P < 0.05$, ** $P < 0.01$ (one-way analysis of variance followed by Student-Newman-Keuls method). DAPI: 4', 6-Diamidino-2-phenylindole; DG: dentate gyrus; GFAP: glial fibrillary acidic protein; LPS: lipopolysaccharides; PBS: phosphate-buffered saline; PTBP-1: polypyrimidine tract-binding protein-1; TUJ-1: neuron-specific class III β -tubulin; UC-MSCs: umbilical cord-derived mesenchymal stem cells.

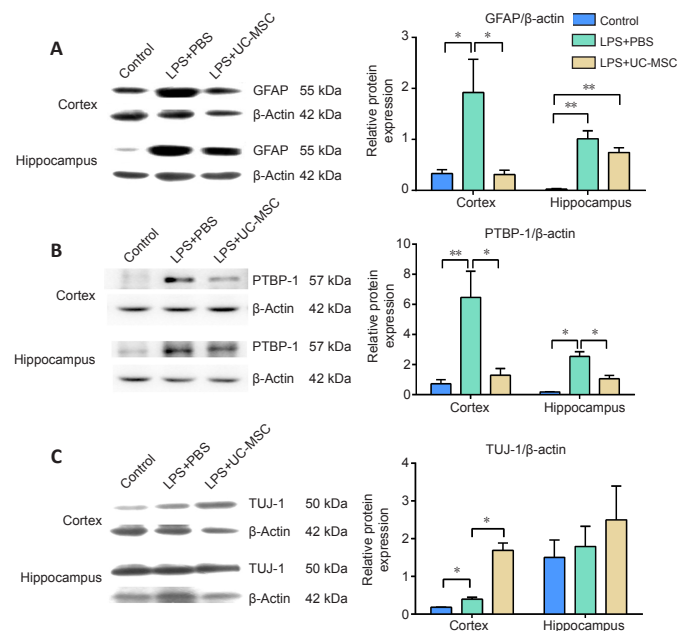


Figure 9 | Effect of UC-MSCs on the protein expression of GFAP (A), PTBP-1 (B), and TUJ-1 (C) in the cortex and hippocampus of neonatal rats with maternal immune activation-associated neonatal brain injury.

Western blot analysis (left) was quantified (right). Data are expressed as mean \pm SEM ($n = 3$). * $P < 0.05$, ** $P < 0.01$ (one-way analysis of variance followed by Student-Newman-Keuls method). DAPI: 4', 6-Diamidino-2-phenylindole; DG: dentate gyrus; GFAP: glial fibrillary acidic protein; LPS: Lipopolysaccharides; PBS: phosphate-buffered saline; PTBP-1: polypyrimidine tract-binding protein-1; TUJ-1: neuron-specific class III β -tubulin; UC-MSCs: umbilical cord-derived mesenchymal stem cells.

The results of several behavioral experiments, including the Morris water maze test and the open field test, showed a lack of spatial exploration and memory abilities after MIA. This finding is consistent with previous studies related to LPS-induced cognitive deficits, which have been shown to induce hippocampal damage (Li et al., 2017b). Using confocal microscopy, we also found many GFAP-positive cells and high expression levels of inflammatory factors (IL-1 β , IL-6) related to this inflammatory injury. It is important to note, however, that the higher IL-6 expression levels in the LPS group were not significantly different from those in the control group, possibly because of the subsiding of inflammatory factors by 40 days after birth (Szot et al., 2017). The LPS dose we used was 0.5 mg/kg, which is similar to Gilmore's experimental dose, taking into account the survival rate and the expression of GFAP and inflammatory factors in the LPS group (Gilmore et al., 2003; Wang et al., 2006).

The mechanisms by which A1 astrocytes become activated and promote regeneration may be involved in the regulation of PTBP-1. In this study, we innovatively explored the relationship between PTBP-1 expression and the activation of GFAP-positive DAAs in this MIA-related neurodevelopmental brain injury model. Our results support previous evidence that LPS-induced MIA triggers an immune response and leads to behavioral damage in fetuses, with a focus on PTBP-1 expression in the CA1, CA3, and DG regions of the hippocampus and the cortex. The lateral and medial EC transmits nonspatial "what" information and spatial "where" information to the hippocampal CA1 region via the indirect pathway of EC layer 2→DG of the hippocampus→CA3→CA1 and the direct pathway of EC layer→CA1, respectively (van Strien et al., 2009). These two different efferent synaptic pathways, known as the perforant path and the temporoammonic path, are associated with the spatial sense and the ability to explore memory (Li et al., 2017c). In this study, we found that the expression of PTBP-1 and GFAP was distributed in the hippocampal CA3 and DG regions along the hippocampal projection circuits in both the LPS + USC-MSC and LPS + PBS groups, suggesting that PTBP-1-regulated inflammatory damage and repair may take place around the hippocampal indirect projection circuit.

We also investigated morphological and behavioral abnormalities in pups with LPS-induced MIA brain injury and validated the efficacy of intranasally administered UC-MSCs. After UC-MSC treatment, the GFAP, PTBP-1, and IL-1 β expression levels were either decreased, or their high expression sites were redistributed, suggesting that PTBP-1 may be involved in the inflammatory response and in GFAP-positive astrocyte activation. We speculate that UC-MSCs may reduce the induction of type A1 astrocytes by inhibiting the nuclear translocation of NF- κ B p65. There is also evidence that MSC-derived exosomes can effectively activate the Wnt/ β -catenin signaling pathway through transplanted A1-type astrocytes (Li et al., 2019). The TUJ-1 expression patterns suggest that this relative decrease in PTBP-1 expression may be involved in the process of dynamic transdifferentiation of astrocytes or in the plasticity repair of neurons; however, these specific processes require further study.

Here, we attempted to show that PTBP-1 may be a key factor in the regulation of brain inflammatory damage by DAAs, as well as neuronal regeneration and neuroplasticity repair after MIA during pregnancy under both physiological and pathological conditions. The correlation may not be a direct cause-and-effect relationship. In the latest neurodegenerative disease model studies, PTBP-1 protein expression sites have been shown to be distributed around dopaminergic neurons in the midbrain, with expression levels closely related to the number of GFAP-positive astrocytes. It has been speculated that PTBP-1 is a key factor in transdifferentiation of astrocytes into neurons (Qian et al., 2020). This process, called "glia-to-neuron conversion", may be an important step in the repair of many types of nerve injury (Russo et al., 2021), and may involve PTBP-1 protein as a key participant (Zhou et al., 2020). In our study, immunohistochemistry, immunofluorescence, and western blotting showed higher PTBP-1 expression levels in activated astrocyte aggregation sites in this neurodevelopmental model after MIA injury.

Our research also supports previous evidence related to the therapeutic effectiveness of stem cells, especially their anti-inflammatory effects and the feasibility of their intranasal delivery into the brain (Jiao et al., 2019, 2021). Previous studies have reported that MSCs and MSC-derived exosomes can inhibit brain inflammation caused by astrocytes, improving symptoms of learning and memory impairments induced by hippocampal injury (Xian et al., 2019; Kim et al., 2020). In this study, we demonstrated that intranasal delivery of UC-MSCs is a relatively simple, noninvasive, reproducible, and effective method for reducing inflammation, which is consistent with previous studies using intravenous administration (Jiang et al., 2011; Donega et al., 2014; Girard et al., 2017). Repair of brain injury by MSCs is currently believed to be more closely related to the regulation of inflammatory factors rather than the direct differentiation of MSCs, because it is easier for these cells to differentiate into bone, cartilage, and other mesodermal tissues (Vidoni et al., 2019). Previous studies have shown that the presence of activated microglia in the brain is closely related to the levels of systemic inflammatory factors (Yang et al., 2013; Son et al., 2017). Moreover, UC-MSCs can reduce inflammation by prompting microglial M2 polarization in a peroxisome proliferator-activated receptor γ -dependent manner (Dabrowska et al., 2019; Gao et al., 2019).

There were several limitations to our study that should be noted. Our experiments did not show that the UC-MSCs reached the specific brain injury site and traced trajectory after administration. LPS-induced brain inflammation-related injury sites in young rats are widespread and the location of stem cells based on chemotaxis may not be unique or

representative. Additionally, more convincing evidence points out that the repair effect of MSCs against neuroinflammation is achieved through paracrine exosomes (Ophelders et al., 2016; Qiu et al., 2018). Our study demonstrated the repair effect by comparing the protein expression differences in GFAP and PTBP-1 before and after UC-MSCs delivery, however we plan to explore the method of labeling exosomes/vesicles in future research. The method of administration in our study is similar to that of Fransson et al. (2014). The brain localization of central nervous system-targeted MSCs in naive mice following intranasal delivery has been shown (Rodríguez-Frutos et al., 2016; Guo et al., 2019; Farfán et al., 2020; Losurdo et al., 2020). Human MSCs were instilled via intranasal administration and the distribution of green fluorescent protein or human nuclei immunofluorescence was observed in the internal plexiform layer of the olfactory bulb ectorhinal cortex and Purkinje cells in the cerebellum of the brain of naive mice 24 hours after delivery. Most of the implanted cells were distributed in the olfactory bulb and midbrain after 7 days of administration (Yu-Taeger et al., 2019). Danielyan et al. (2011, 2014) have shown that 3% of administered cell nuclear antigen-positive EGFP-MSCs were proliferative 4.5 months after application and did not exceed 1% in peripheral organs. To date, PTBP-1 and GFAP protein expression levels have mainly been studied in models of aging. Studies related to the mechanisms of astrocyte transdifferentiation, neuronal plasticity repair, and brain development after MIA injury are still limited, and future studies are required to reach more definitive conclusions. Additionally, the inflammation in the brain may not be determined by astrocytes alone, but also by the participation of microglia and other inflammatory factors. It is also widely accepted that microglial responses after injury can lead to inflammation in the brain, and the connections and mechanisms by which astrocytes and microglia respond after injury remain to be further elucidated. Finally, perinatal cerebral ischemia and hypoxic injuries are major causes of NBI. Studies have confirmed that the neuroinflammatory response is closely related to the presence of cerebral ischemia and hypoxic damage, and further research should focus on models of ischemic and hypoxic damage.

In summary, PTBP-1 may be a key protein in the regulation of LPS-induced MIA, which leads to NBI. Intranasally delivered stem cells regulated the number and function of GFAP-positive astrocytes by inhibiting PTBP-1 expression, alleviating inflammatory damage in the brain, promoting plastic regeneration of neurons, and improving brain function. This study investigated PTBP-1 in an animal model of developmental brain injury to evaluate stem cell therapy. These findings provide promising new directions for research; however, the underlying mechanisms need further exploration.

Acknowledgments: We thank the administrative staff and associates from Dalian Medical University, Liaoning Normal University and Dalian Innovation Institute of Stem Cell and Precision Medicine for their work on behalf of this study.

Author contributions: Study conception and design: JL, WZ; data acquisition, analysis, or interpretation: YJ, LNZ, NFC, YTS; statistical analysis and manuscript drafting: YJ, YTS; fundamental experiment study: JL, WZ, YJ, NFC, XLJ, YCW, WJW, CH; behavioral experiment: YTS, LNZ, JYW, XLJ, NFC; sample preparation and processing: CH, YCW; cell preparation: XG, WJW; study supervision: JL. All authors reviewed and approved the final version of the manuscript.

Conflicts of interest: We have declared no conflict of interest.

Editor note: JL is an Editorial Board member of Neural Regeneration Research. She was blinded from reviewing or making decisions on the manuscript. The article was subject to the journal's standard procedures, with peer review handled independently of this Editorial Board member and their research groups.

Availability of data and materials: All data generated or analyzed during this study are included in this published article and its supplementary information files.

Open access statement: This is an open access journal, and articles are distributed under the terms of the Creative Commons AttributionNonCommercial-ShareAlike 4.0 License, which allows others to remix, tweak, and build upon the work non-commercially, as long as appropriate credit is given and the new creations are licensed under the identical terms.

Additional file:

Additional file 1: Informed consent form (Chinese).

References

- Bergdolt L, Dunaevesky A (2019) Brain changes in a maternal immune activation model of neurodevelopmental brain disorders. *Prog Neurobiol* 175:1-19.
- Brown AS (2011) The environment and susceptibility to schizophrenia. *Prog Neurobiol* 93:23-58.
- Burd I, Balakrishnan B, Kannan S (2012) Models of fetal brain injury, intrauterine inflammation, and preterm birth. *Am J Reprod Immunol* 67:287-294.
- Burda JE, Bernstein AM, Sofroniew MV (2016) Astrocyte roles in traumatic brain injury. *Exp Neurol* 275 Pt 3:305-315.
- Canetta S, Bolkan S, Padilla-Coreano N, Song LJ, Sahn R, Harrison NL, Gordon JA, Brown A, Kellendonk C (2016) Maternal immune activation leads to selective functional deficits in offspring parvalbumin interneurons. *Mol Psychiatry* 21:956-968.
- Canetta SE, Bao Y, Co MD, Ennis FA, Cruz J, Terajima M, Shen L, Kellendonk C, Schaefer CA, Brown AS (2014) Serological documentation of maternal influenza exposure and bipolar disorder in adult offspring. *Am J Psychiatry* 171:557-563.
- Chávez CE, Oyarzún JE, Avendaño BC, Mellado LA, Inostroza CA, Alvear TF, Orellana JA (2019) The opening of connexin 43 hemichannels alters hippocampal astrocyte function and neuronal survival in prenatally LPS-exposed adult offspring. *Front Cell Neurosci* 13:460.

- Chen SY, Lin MC, Tsai JS, He PL, Luo WT, Herschman H, Li HJ (2019) EP(4) Antagonist-elicited extracellular vesicles from mesenchymal stem cells rescue cognition/learning deficiencies by restoring brain cellular functions. *Stem Cells Transl Med* 8:707-723.
- Cui Y, Ma S, Zhang C, Cao W, Liu M, Li D, Lv P, Xing Q, Qu R, Yao N, Yang B, Guan F (2017) Human umbilical cord mesenchymal stem cells transplantation improves cognitive function in Alzheimer's disease mice by decreasing oxidative stress and promoting hippocampal neurogenesis. *Behav Brain Res* 320:291-301.
- Dabrowska S, Andrzejewska A, Lukomska B, Janowski M (2019) Neuroinflammation as a target for treatment of stroke using mesenchymal stem cells and extracellular vesicles. *J Neuroinflammation* 16:178.
- Danielyan L, Beer-Hammer S, Stolzing A, Schäfer R, Siegel G, Fabian C, Kahle P, Biedermann T, Lourhmati A, Buadze M, Novakovic A, Proksch B, Gleiter CH, Frey WH, Schwab M (2014) Intranasal delivery of bone marrow-derived mesenchymal stem cells, macrophages, and microglia to the brain in mouse models of Alzheimer's and Parkinson's disease. *Cell Transplant* 23 Suppl 1:S123-139.
- Danielyan L, Schäfer R, von Ameln-Mayerhofer A, Bernhard F, Verleysdonk S, Buadze M, Lourhmati A, Klopfer T, Schaumann F, Schmid B, Koehle C, Proksch B, Weissert R, Reichardt HM, van den Brandt J, Buniatian GH, Schwab M, Gleiter CH, Frey WH, 2nd (2011) Therapeutic efficacy of intranasally delivered mesenchymal stem cells in a rat model of Parkinson disease. *Rejuvenation Res* 14:3-16.
- Dominici M, Le Blanc K, Mueller I, Slaper-Cortenbach I, Marini F, Krause D, Deans R, Keating A, Prockop D, Horwitz E (2006) Minimal criteria for defining multipotent mesenchymal stromal cells. The International Society for Cellular Therapy position statement. *Cytotherapy* 8:315-317.
- Donega V, Nijboer CH, van Tilborg G, Dijkhuizen RM, Kavelaars A, Heijnen CJ (2014) Intranasally administered mesenchymal stem cells promote a regenerative niche for repair of neonatal ischemic brain injury. *Exp Neurol* 261:53-64.
- Drommelschmidt K, Serdar M, Bendix I, Herz J, Bertling F, Prager S, Keller M, Ludwig AK, Duhan V, Radtke S, de Miroschedji K, Horn PA, van de Looij Y, Giebel B, Felderhoff-Müser U (2017) Mesenchymal stem cell-derived extracellular vesicles ameliorate inflammation-induced preterm brain injury. *Brain Behav Immun* 60:220-232.
- Estes ML, McAllister AK (2016) Maternal immune activation: Implications for neuropsychiatric disorders. *Science* 353:772-777.
- Faezi M, Nasseri Maleki S, Aboutaleb N, Nikogoftar M (2018) The membrane mesenchymal stem cell derived conditioned medium exerts neuroprotection against focal cerebral ischemia by targeting apoptosis. *J Chem Neuroanat* 94:21-31.
- Farfán N, Carril J, Redel M, Zamorano M, Araya M, Monzón E, Alvarado R, Contreras N, Tapiabustos A, Quintanilla ME, Ezquer F, Valdés JL, Israel Y, Herrera-Marschitz M, Morales P (2020) Intranasal administration of mesenchymal stem cell secretome reduces hippocampal oxidative stress, neuroinflammation and cell death, improving the behavioral outcome following perinatal asphyxia. *Int J Mol Sci* 21:7800.
- Fragopoulou AF, Qian Y, Heijt RD, Forsberg H (2019) Can neonatal systemic inflammation and hypoxia yield a cerebral palsy-like phenotype in periparturient mice? *Mol Neurobiol* 56:6883-6900.
- Fransson M, Piras E, Wang H, Burman J, Duprez I, Harris RA, LeBlanc K, Magnusson PU, Brittebo E, Loskog AS (2014) Intranasal delivery of central nervous system-retargeted human mesenchymal stromal cells prolongs treatment efficacy of experimental autoimmune encephalomyelitis. *Immunology* 142:431-441.
- Gao J, Cheng Y, Hao H, Yin Y, Xue J, Zhang Q, Li L, Liu J, Xie Z, Yu S, Li B, Han W, Mu Y (2019) Decitabine assists umbilical cord-derived mesenchymal stem cells in improving glucose homeostasis by modulating macrophage polarization in type 2 diabetic mice. *Stem Cell Res Ther* 10:259.
- García-Blanco MA, Jamison SF, Sharp PA (1989) Identification and purification of a 62,000-dalton protein that binds specifically to the polypyrimidine tract of introns. *Genes Dev* 3:1874-1886.
- Gascón S, Masserdotti G, Russo GL, Götz M (2017) Direct neuronal reprogramming: achievements, hurdles, and new roads to success. *Cell Stem Cell* 21:18-34.
- Gilmore JH, Jarskog LF, Vadlamudi S (2003) Maternal infection regulates BDNF and NGF expression in fetal and neonatal brain and maternal-fetal unit of the rat. *J Neuroimmunol* 138:49-55.
- Girard SD, Virard I, Lacassagne E, Paumier JM, Lahlou H, Jabes F, Molino Y, Stephan D, Baranger K, Belghazi M, Deveze A, Khrestchatsky M, Nivet E, Roman FS, Féron F (2017) From blood to lesioned brain: an in vitro study on migration mechanisms of human nasal olfactory stem cells. *Stem Cells Int* 2017:1478606.
- Guo S, Perets N, Betzer O, Ben-Shaul S, Sheinin A, Michalevski I, Popovtzer R, Offen D, Levenberg S (2019) Intranasal delivery of mesenchymal stem cell derived exosomes loaded with phosphatase and tensin homolog sirna repairs complete spinal cord injury. *ACS Nano* 13:10015-10028.
- Habib N, McCabe C, Medina S, Varshavsky M, Kitsberg D, Dvir-Szternfeld R, Green G, Dionne D, Nguyen L, Marshall JL, Chen F, Zhang F, Kaplan T, Regev A, Schwartz M (2020) Disease-associated astrocytes in Alzheimer's disease and aging. *Nat Neurosci* 23:701-706.
- Hampel H, Caraci F, Cuello AC, Caruso G, Nisticò R, Corbo M, Baldacci F, Toschi N, Garaci F, Chiesa PA, Verdooner SR, Akman-Anderson L, Hernández F, Ávila J, Emanuele E, Valenzuela PL, Lucía A, Watling M, Imbimbo BP, Vergallo A, et al. (2020) A path toward precision medicine for neuroinflammatory mechanisms in Alzheimer's disease. *Front Immunol* 11:456.
- Harvey L, Boksa P (2012) Prenatal and postnatal animal models of immune activation: relevance to a range of neurodevelopmental disorders. *Dev Neurobiol* 72:1335-1348.
- Imai K, Kotani T, Tsuda H, Nakano T, Ushida T, Iwase A, Nagai T, Toyokuni S, Suzumura A, Kikkawa F (2018) Administration of molecular hydrogen during pregnancy improves behavioral abnormalities of offspring in a maternal immune activation model. *Sci Rep* 8:9221.
- Jiang Y, Zhu J, Xu G, Liu X (2011) Intranasal delivery of stem cells to the brain. *Expert Opin Drug Deliv* 8:623-632.
- Jiao Y, Li XY, Liu J (2019) A new approach to cerebral palsy treatment: discussion of the effective components of umbilical cord blood and its mechanisms of action. *Cell Transplant* 28:497-509.
- Jiao Y, Liu YW, Chen WG, Liu J (2021) Neuroregeneration and functional recovery after stroke: advancing neural stem cell therapy toward clinical application. *Neural Regen Res* 16:80-92.
- Kim S, Kim YE, Hong S, Kim KT, Sung DK, Lee Y, Park WS, Chang YS, Song MR (2020) Reactive microglia and astrocytes in neonatal intraventricular hemorrhage model are blocked by mesenchymal stem cells. *Glia* 68:178-192.
- Lei J, Liu X, Song M, Zhou Y, Fan J, Shen X, Xu X, Kapoor I, Zhu G, Wang J (2020) Aberrant exon 8/8a splicing by downregulated ptpb (polypyrimidine tract-binding protein) 1 increases ca(v)1.2 dihydropyridine resistance to attenuate vasodilation. *Arterioscler Thromb Vasc Biol* 40:2440-2453.
- Li B, Concepcion K, Meng X, Zhang L (2017a) Brain-immune interactions in perinatal hypoxic-ischemic brain injury. *Prog Neurobiol* 159:50-68.
- Li C, Jiao G, Wu W, Wang H, Ren S, Zhang L, Zhou H, Liu H, Chen Y (2019) Exosomes from bone marrow mesenchymal stem cells inhibit neuronal apoptosis and promote motor function recovery via the Wnt/ β -catenin signaling pathway. *Cell Transplant* 28:1373-1383.
- Li M, Li C, Yu H, Cai X, Shen X, Sun X, Wang J, Zhang Y, Wang C (2017b) Lentivirus-mediated interleukin-1 β (IL-1 β) knock-down in the hippocampus alleviates lipopolysaccharide (LPS)-induced memory deficits and anxiety- and depression-like behaviors in mice. *J Neuroinflammation* 14:190.
- Li Y, Xu J, Liu Y, Zhu J, Liu N, Zeng W, Huang N, Rasch MJ, Jiang H, Gu X, Li X, Luo M, Li C, Teng J, Chen J, Zeng S, Lin L, Zhang X (2017c) A distinct entorhinal cortex to hippocampal CA1 direct circuit for olfactory associative learning. *Nat Neurosci* 20:559-570.
- Liddelov SA, Guttenplan KA, Clarke LE, Bennett FC, Bohlen CJ, Schirmer L, Bennett ML, Münch AE, Chung WS, Peterson TC, Wilton DK, Frouin A, Napier BA, Panicker N, Kumar M, Buckwalter MS, Rowitch DH, Dawson VL, Dawson TM, Stevens B, et al. (2017) Neurotoxic reactive astrocytes are induced by activated microglia. *Nature* 541:481-487.
- Losurdo M, Pedrazzoli M, D'Agostino C, Elia CA, Massenzio F, Lonati E, Mauri M, Rizzi L, Molteni L, Bresciani E, Dander E, D'Amico G, Bulbarelli A, Torsello A, Matteoli M, Buffelli M, Coco S (2020) Intranasal delivery of mesenchymal stem cell-derived extracellular vesicles exerts immunomodulatory and neuroprotective effects in a 3xTg model of Alzheimer's disease. *Stem Cells Transl Med* 9:1068-1084.
- Muhammad T, Ikram M, Ullah R, Rehman SU, Kim MO (2019) Hesperetin, a citrus flavonoid, attenuates LPS-induced neuroinflammation, apoptosis and memory impairments by modulating TLR4/NF- κ B signaling. *Nutrients* 11:648.
- Mwaniki MK, Atieno M, Lawn JE, Newton CR (2012) Long-term neurodevelopmental outcomes after intruterine and neonatal insults: a systematic review. *Lancet* 379:445-452.
- Ophelders DR, Wolfs TG, Jellema RK, Zwanenburg A, Andriessen P, Delhaas T, Ludwig AK, Radtke S, Peters V, Janssen L, Giebel B, Kramer BW (2016) Mesenchymal stromal cell-derived extracellular vesicles protect the fetal brain after hypoxia-ischemia. *Stem Cells Transl Med* 5:754-763.
- Pierrat V, Marchand-Martin L, Arnaud C, Kaminski M, Resche-Rigon M, Lebeaux C, Bodeau-Livinec F, Morgan AS, Goffinet F, Marret S, Ancel PY, EPIPAGE-2 writing group (2017) Neurodevelopmental outcome at 2 years for preterm children born at 22 to 34 weeks' gestation in France in 2011: EPIPAGE-2 cohort study. *BMJ* 358:j3448.
- Purves-Tyson TD, Weber-Stadlbauer U, Richetto J, Rothmond DA, Labouesse MA, Polesel M, Robinson K, Shannon Weickert C, Meyer U (2021) Increased levels of midbrain immune-related transcripts in schizophrenia and in mice offspring after maternal immune activation. *Mol Psychiatry* 26:849-863.
- Qian H, Kang X, Hu J, Zhang D, Liang Z, Meng F, Zhang X, Xue Y, Maimon R, Dowdy SF, Devaraj NK, Zhou Z, Mobley WC, Cleveland DW, Fu XD (2020) Reversing a model of Parkinson's disease with in situ converted nigral neurons. *Nature* 582:550-556.
- Qiu G, Zeng G, Ge M, Wang J, Huang R, Shu Q, Xu J (2018) Mesenchymal stem cell-derived extracellular vesicles affect disease outcomes via transfer of microRNAs. *Stem Cell Res Ther* 9:320.
- Ravichandran VA, Kim M, Han SK, Cha YS (2018) Stachys sieboldii extract supplementation attenuates memory deficits by modulating BDNF-CREB and its downstream molecules, in animal models of memory impairment. *Nutrients* 10:917.
- Rodríguez-Frutos B, Otero-Ortega L, Gutiérrez-Fernández M, Fuentes B, Ramos-Cejudo J, Díez-Tejedor E (2016) Stem cell therapy and administration routes after stroke. *Transl Stroke Res* 7:378-387.
- Russo GL, Sonsalla G, Natarajan P, Breunig CT, Bulli G, Merl-Pham J, Schmitt S, Giehrh-Schwab J, Giesert F, Jastroch M, Zischka H, Wurst W, Stricker SH, Hauck SM, Masserdotti G, Götz M (2021) CRISPR-mediated induction of neuron-enriched mitochondrial proteins boosts direct glia-to-neuron conversion. *Cell Stem Cell* 28:524-534.e7.
- Son M, Oh S, Park H, Ahn H, Choi J, Kim H, Lee HS, Lee S, Park HJ, Kim SU, Lee B, Byun K (2017) Protection against RAGE-mediated neuronal cell death by sRAGE-secreting human mesenchymal stem cells in 5xFAD transgenic mouse model. *Brain Behav Immun* 66:347-358.
- Sturman O, Germain PL, Bohacek J (2018) Exploratory rearing: a context- and stress-sensitive behavior recorded in the open-field test. *Stress* 21:443-452.
- Szot P, Franklin A, Figlewicz DP, Beuca TP, Bullock K, Hansen K, Banks WA, Raskind MA, Peskind ER (2017) Multiple lipopolysaccharide (LPS) injections alter interleukin 6 (IL-6), IL-7, IL-10 and IL-6 and IL-7 receptor mRNA in CNS and spleen. *Neuroscience* 355:9-21.
- Thomi G, Surbek D, Haesler V, Joergers-Messerli M, Schoeberlein A (2019a) Exosomes derived from umbilical cord mesenchymal stem cells reduce microglia-mediated neuroinflammation in perinatal brain injury. *Stem Cell Res Ther* 10:105.
- Thomi G, Joergers-Messerli M, Haesler V, Muri L, Surbek D, Schoeberlein A (2019b) Intranasally administered exosomes from umbilical cord stem cells have preventive neuroprotective effects and contribute to functional recovery after perinatal brain injury. *Cells* 8:855.
- van Strien NM, Cappaert NL, Witter MP (2009) The anatomy of memory: an interactive overview of the parahippocampal-hippocampal network. *Nat Rev Neurosci* 10:272-282.
- Vidoni C, Ferraresi A, Secomandi E, Vallino L, Gardin C, Zavan B, Mortellaro C, Isidoro C (2019) Autophagy drives ontogenic differentiation of human gingival mesenchymal stem cells. *Cell Commun Signal* 17:98.
- Vismara I, Papa S, Veneruso V, Mauri E, Mariani A, De Paola M, Affatato R, Rossetti A, Sponchioni M, Mascatelli D, Sacchetti A, Rossi F, Forloni G, Veglianesi P (2020) Selective modulation of α 1 astrocytes by drug-loaded nano-structured gel in spinal cord injury. *ACS Nano* 14:360-371.
- Wang X, Rousset CI, Hagberg H, Mallard C (2006) Lipopolysaccharide-induced inflammation and perinatal brain injury. *Semin Fetal Neonatal Med* 11:343-353.
- Wang X, Wang L, Yu X, Li Y, Liu Z, Zou Y, Zheng Y, He Z, Wu H (2019) Glutaminyl cyclase inhibitor exhibits anti-inflammatory effects in both AD and LPS-induced inflammatory model mice. *Int Immunopharmacol* 75:105770.
- Xian P, Hei Y, Wang R, Wang T, Yang J, Li J, Di Z, Liu Z, Baskys A, Liu W, Wu S, Long Q (2019) Mesenchymal stem cell-derived exosomes as a nanotherapeutic agent for amelioration of inflammation-induced astrocyte alterations in mice. *Theranostics* 9:5956-5975.
- Xu J, Feng Z, Wang X, Xiong Y, Wang L, Ye L, Zhang H (2019) hUC-MSCs exert a neuroprotective effect via anti-apoptotic mechanisms in a neonatal HIE rat model. *Cell Transplant* 28:1552-1559.
- Yang H, Yang H, Xie Z, Wei L, Bi J (2013) Systemic transplantation of human umbilical cord derived mesenchymal stem cells-educated T regulatory cells improved the impaired cognition in ABPPsw/PS1dE9 transgenic mice. *PLoS One* 8:e69129.
- Yu-Taeger L, Stricker-Shaver J, Arnold K, Bamynek-Dziuk P, Novati A, Singer E, Lourhmati A, Fabian C, Mags J, Riess O, Schwab M, Stolzing A, Danielyan L, Nguyen HHP (2019) Intranasal administration of mesenchymal stem cells ameliorates the abnormal dopamine transmission system and inflammatory reaction in the R6/2 mouse model of huntington disease. *Cells* 8:595.
- Zhou H, Su J, Hu X, Zhou C, Li H, Chen Z, Xiao Q, Wang B, Wu W, Sun Y, Zhou Y, Tang C, Liu F, Wang L, Feng C, Liu M, Li S, Zhang Y, Xu H, Yao H, et al. (2020) Glia-to-neuron conversion by CRISPR-CasRx alleviates symptoms of neurological disease in mice. *Cell* 181:590-603.e16.

C-Editor: Zhao M; S-Editors: Yu J, Li CH; L-Editors: Bell M, Song LP; T-Editor: Jia Y